SUM4Re

Creating materials banks
from digital urban mining

D2.4 MFT methodological framework acquisition

VERSION 1.0

28 October 2025

PUBLIC

Associated with document Ref. 101129961

Funded by the European Union. Views and opinions expressed are however those of the author(s) only and do not necessarily reflect those of the European Union. Neither the European Union nor the granting authority can be held responsible for them.

Funded by the European Union

SUM4Re

Creating materials banks from digital urban mining

Deliverable ID	D2.4
Deliverable name	MFT methodological framework acquisition
Lead partner	GSCAN
Contributors	CTH

PUBLIC

Funded by the European Union

DOCUMENT INFORMATION

Document name	D2.4 MFT methodological framework acquisition
Version	1.0
Due date	31/10/2025
Report date	28/10/2025
Number of pages	32
Lead Author	Sander Sein (GSCAN)
Other Authors	-
Dissemination level	Public

REVISION HISTORY

Rev.	Date	Description of revision
0.1	09/10/2025	Initial version
0.2	24/10/2025	Reviewed version
1.0	28/10/2025	Final version (approved)

DOCUMENT APPROVAL

Written	Sander Sein (GSCAN)	09/10/2025/
Revised	Jesús Balado (UVIGO), Jon Zubizarreta (MOYUA)	13/10/2025
	Ana Sánchez (UVIGO, Project Manager)	28/10/2025
Approved	Pedro Arias Sánchez (UVIGO, Project Coordinator)	28/10/2025

EXECUTIVE SUMMARY

This deliverable, D2.4 "Data collection for complex or concealed elements with MFT," details the progress and results of Task 2.4 within the SUM4Re project.

It focuses on the application of Muon Flux Technology (MFT) for detailed assessment of structures, providing 3D information for Building Information Modeling (BIM) that other technologies cannot. The task involved extensive model-based simulations using GEANT4, incorporating cosmic particle sources like CRY and MPS, to simulate realistic particle transport and detection. These simulations were crucial for developing and testing various reconstruction algorithms, including particle track filtering, ray casting, and volume density map generation.

Furthermore, the deliverable describes the validation testing of different materials to enhance the confidence in the developed reconstruction and material classification algorithms. The findings and developed algorithms will be directly utilized in Task 10.2 for case study measurements in The Hague.

The document also addresses the state of the art, relevance to other Work Packages, legal considerations, and identifies target materials for investigation, such as plain concrete, reinforced concrete with various defects, steel, and timber.

GLOSSARY

Terms, Abbreviations, and Acronyms

AI	Artificial Intelligence
C-BIM	Circular BIM
CRY	Cosmic-ray shower generator
DAQ	Data acquisistion
EC	European Comission
FIB	International Federation for Structural Concrete
GEANT4	GEometry ANd Tracking software
GPR	Ground Penetrating Radar
MPS	Muon Parametrisation Source
MCNPX	Monte Carlo N-Particle eXtended
MFT	Muon Flux Technology
SUM4Re	Creating material banks from digital urban mining (project name)
WA	Work Area
WP	Work Package

TABLE OF CONTENTS

DOCUMENT INFORMATION **3**
REVISION HISTORY **3**
DOCUMENT APPROVAL **3**
EXECUTIVE SUMMARY **4**
GLOSSARY **5**
TABLE OF CONTENTS **6**
LIST OF TABLES **7**
LIST OF FIGURES **8**
1. INTRODUCTION **9**
1.1. SUM4Re RESEARCH CONTEXT AND APPROACH 9
1.2. SCOPE AND PURPOSE OF DELIVERABLE D2.4 9
2. RESEARCH APPROACH **10**
2.1. STATE OF THE ART 10
2.2. RELEVANCE TO THE WP2 OBJECTIVES 11
2.3. RELEVANCE TO THE OTHER WP OBJECTIVES 11
2.4. LEGAL CONSIDERATIONS 11
2.5. TARGET MATERIALS 12
3. TECHNICAL BRIEF **13**
3.1. SIMULATION ENVIRONMENT GEANT4 13
3.2. EQUIPMENT TECHNICAL SPECIFICATION 14
3.3. DATA ACQUISITION PROCESS 15
4. DEVELOPMENT **17**
4.1. HUMAN RESOURCES ASSIGNMENT AND ROLES 17
4.2. SCHEDULING 17
4.3. CRITICAL TASKS AND MILESTONES 18
4.3.1. Critical Tasks *18*
4.3.2. Milestones *18*
4.4. SIMULATION STUDY 18
4.5. REAL MATERIAL TESTING WITH RESPECT TO APPLICATION AND UTILIZATION 23
5. CHALLENGES AND LIMITATIONS **26**
5.1. TECHNICAL CONSTRAINTS OF THE TECHNOLOGY 26
5.1.1. Hardware *27*
5.1.2. Data acquisition *27*
5.1.3. Data processing *27*
6. CONCLUSION **29**
7. BIBLIOGRAPHY **30**

LIST OF TABLES

Table 1. Human resources 17

Table 2. Chemical composition of CEM I plain concrete and change of composition for different degradation processes 21

LIST OF FIGURES

Figure 1. The distribution of atmospheric ray muons and electrons as a function of the intrinsic scattering angle θ in the hodoscope (from the Geant4 model with the CRY event generator). 13

Figure 2. Comparison of old and new generation tomographic scanner setup 14

Figure 3. Scanner TLL in the production facility 15

Figure 4. Scattering angle distribution of 0 – 0,5 GeV muons through plain concrete and concrete with 10 mm rebar. 19

Figure 5. Scattering angle differences of 0 – 0,5 GeV muons through plain concrete, concrete with 10 mm rebar, 10 mm rebar with 5 mm rust and fully rusted. 19

Figure 6. Scattering angle differences of 0 – 0.5 GeV Muons in 500 mm block 20

Figure 7. Scattering angle differences of 0.5 – 1.5 GeV Muons in 500 mm block 20

Figure 8. Scattering angle differences of 1.5 - 3.0 GeV Muons in 500 mm block 21

Figure 9. Scattering angle differences of 0-0.5 and 0.5 - 1.5 GeV Muons in 1000 mm block with different degradation processes. 22

Figure 10. Rebars in 1000 thick concrete block after 24 h (left) and 120 h (right) exposure time 22

Figure 11. Scanner setup for material validation 23

Figure 12. Air measurements with rhombus shape, which reflects how the muon flux filtering cuts of specific energy levels in reconstruction algorithm. 23

Figure 13. Six concrete cubes in a measurement setup. Experimental run number 17 24

Figure 14. Twelve cubes stacked on top of each other with steel and concrete in a measurement setup. Experimental run number 14 24

Figure 15. Mix of six cubes of different sizes of concrete and steel in a measurement setup. Experimental run number 13 24

Figure 16. Reconstruction results of the measurement setups. Where steel with higher density appear brighter, because it is causing more scattering. 25

Figure 17. Measurement setup with composite and more complex variations of materials. Larger test bodies nr. 1 and 2. have both rebars and post-tensioning ducts inside. 25

Figure 18. Horizontal slice from different heights of the measurement of composite and more complex variations of materials. 26

Figure 19. The outcome of the MFT data 27

1. Introduction

1.1. SUM4Re research context and approach

The SUM4Re project ("Creating material banks from digital urban mining") is a European initiative funded by Horizon Europe (ID 101129961), running from June 2024 to November 2027. Its main goal is to turn construction and demolition waste—the largest waste stream in the EU—into reusable "material banks." This is achieved by combining urban mining (selective reuse), advanced technologies (automated scanning, AI, circular BIM, blockchain), and a systematic approach to identifying, analysing, and tracking materials. Three pilot projects will be carried out in Spain, the Netherlands, and Norway.

The project brings together 17 partners, including universities (coordinated by the University of Vigo), technology centres, and companies in the construction and digitalization sectors. The ultimate objective is to boost circularity in construction through digital tools and open standards—reducing waste, increasing the supply of secondary raw materials, and fostering new business models based on the circular economy.

1.2. Scope and purpose of deliverable D2.4

This deliverable serves to describe the progress made and results achieved for Task 2.4: Data collection for complex or concealed elements with MFT

MFT concept offers a unique datapoint that rival technologies (such as ultrasound, GPR, and X-rays) cannot physically achieve and even provides 3D information for BIM creation in T3.7.

This task will focus on a generation of model-based simulations using GEANT4 (Agostinelli) (for GEomentry ANd Tracking) software platform including cosmic particle sources, such as CRY (Cosmic-ray shower generator) or MPS (Muon Parametrisation Source). In Geant4 the geometry of detection system, volume of interest, varied materials and environment will be accurately described enabling to simulate realistic particle transport and detection. The simulation results will be used for testing different reconstruction algorithms including, particle track filtering, ray castings and volume density maps generation.

In addition, the task involves extensive validation testing of the same materials to increase the confidence of developed reconstruction and material classification algorithms.

The delivered algorithms will be directly used in Task 10.2 Case Study measurement in the Hague.

2. Research approach

GScan is established in 2018, but research activities started already in 2016. Within the nine years, the focus has changed from early-stage feasibility study to fundamental research and technology readiness have been improved with real time measurements since March 2023.

2.1. State of the art

This research is needed to fill the gap, by enabling detailed assessment of any structure thanks to high penetration rate combined with a high level of accuracy. It can provide additional added value for the customers by mapping internal structures and identifying materials allowing to get an accurate overview of the current condition.

The gap is existing due to complexity of determining the exact condition of reinforced concrete, which has relatively high density and inhomogeneity. The variety in composition and amount of reinforcement makes it hard to determine the degradation processes and whole internal geometry.

Currently, the volumetric inspections are a combination of non-destructive and destructive methods. Most common methods are gamma radiography, ground penetrating radars (GPR) and ultrasound mapping.

- Gamma rays and X-rays are reliable and easily interpretable, but they are hazardous and have penetration depth only up to 300 mm. (Geraldo)
- Ground penetrating radars (GPR) enable quick and universal data collection of structures and soil depending on the frequency of the antenna. The electromagnetic waves are affected by the temperature, moisture and density of materials, which limits the penetration depth. In addition, expert knowledge is needed for performing the measurement and data interpretation. (Jol)
- Ultrasonic mapping offers also quick data collection, but have similar limitations as GPR with having the need for expert knowledge for measurements and interpretation, while the penetration depth is limited to 800 mm.

The data collection is just the first step in the condition assessment. The analysis and further modelling are still very subjective and qualitative or at best semi-quantitative. An essential element of the decision-making process of hidden or concealed elements is the uncertainty as to whether the final decision will lead to the best outcome. This uncertainty comes from the fact that it is not possible to predict or model accurately the scenarios that will be derived from decisions. Therefore, engineering is mostly about good enough decisions, grounded on dependable evidence and a scientifically justifiable derivation, and not concerned with correct decisions, since this concept is impossible to assess.

The scientific literature of MFT Is limited, as the first proof of concept was published in 2021 (Niederleithinger) and more robust application in civil engineering was published in 2025 (SEIN). GScan initiated its muon flux technology operations with feasibility studies in 2016 for detecting humans in a passenger car, subsequently introducing the inaugural practical muon tomography solution in 2018. A collaborative effort with the University of Tartu in 2020 resulted in a proof of concept , which demonstrated the capabilities of our hardware and algorithms in differentiating light-element materials, such as concrete and steel, commonly utilized in construction. Since then, extensive R&D collaborations with academic institutions including the University of Louvain, University of Sheffield, University of Exeter, the German Aerospace Center, the Bruno Kessler Foundation and CAEN have been carried out. Most of the methods have been covered with a patent WO2019166669A1 (GEORGADZE). High level functionality can be described as follows.

1. Saved data files from each detector exposure position contain channel activation data from data acquisition (DAQ) electronics, along with metadata detailing hodoscope location in space and exposure duration. This channel activation data is then translated

into local xyz coordinates. A tracking algorithm refines the particle's actual trajectory through the hodoscope and eliminates erroneous channel activations.
2. Following the tracking algorithm, angle filtering removes low-energy particles. All detector position exposures are then consolidated into a single, large virtual detector plane, utilizing the hodoscope's positional metadata.
3. Based on the xyz exposures from the hodoscope's first two plates, the ray is projected into space, assuming the particle trajectory.
4. The processed data is reconstructed using the different voxel sizes: from 10 mm to 1 mm. The larger voxel sizes include more statistics but lack resolution, so the optimal size is currently 3 mm.

In 2021, GScan commenced the development of engineering solutions for tracking technology and software/algorithms using Geant4 simulations. Technical evaluations were also conducted on concrete and reinforced concrete samples.

By late 2022, the pilot production technology was operational, culminating in the creation of our first industrial-scale prototype tracker in March 2023. Measuring submarine nuclear reactors in northern Estonia served to validate the technology's real-world efficacy for internal 3D reconstruction under specific client requirements.

Preparations for outdoor applications also commenced in 2022 through joint projects with Estonian partners AS Teede Tehnokeskus and Enefit Green AS. These projects centered on NDT for reinforced concrete and steel components in wind turbines, supported by financial assistance from the Estonian Business and Innovation Agency.

In June 2023, an integrated prototype tomographic system (a scanner) was successfully constructed. Concurrently, the software team developed the comprehensive system control architecture, encompassing data acquisition, algorithm integration, and a front-end interface, with the prototype finalized by end of 2023.

2.2. Relevance to the WP2 objectives

T2.4 is of special relevance for the development of WP2 and serving as additional source of information of hidden and concealed elements. The technology provides additional information about geometries and materials inside the structures that aren’t visible with other existing technologies investigated in WP2. The technology is used for small area investigations and will be integrated with other technologies through 3d information base.

2.3. Relevance to the other WP objectives

T2.4 serves as a 3D data acquisition that will be the basis of geometric information of hidden elements for the BIM models of the following time tasks. T2.4 is mainly related to:

- **WP3**. Specifically, with T3.4 where the 3D data provided in this task is to train and validate artificial intelligence models.
- **WP6**. T2.4 serves both for the geometric information base of hidden elements and materials to propose Circular-BIM (C-BIM) into GENIA, CIRDAX and COCULAR.
- **WP10**. The methodology and the software developed in T2.4 are necessary for data acquisition in the Netherlands case study.

2.4. Legal considerations

The MFT collects information of natural flux that is affected by materials that are between the detector plates. The data structure is only related to the time and location of muon or other charged particles passing through the detector plate. This information can’t be related to any humans and is not harming privacy.

The data is transferred to GScan server through private connection using commercial service providers. There is a risk of data leakage, but the data is only readable with patentad program. No other risks have been identified related to the MFT application.

2.5. Target materials

The main construction materials are concrete, steel and different combinations of these materials, with all relevant defects and deterioration processes. The list of materials under investigation:

- Plain concrete, thickness varies between 100 mm to 1000 mm.
- Plain concrete with voids
- Plain concrete with cracks
- Plain concrete with delamination
- Rebar, different diameters
- Corroded rebar, different diameters and corrosion severity
- Reinforced concrete with different rebars
- Reinforced concrete with carbonisation
- Reinforced concrete with chlorides
- Reinforced concrete with corroded rebar
- Reinforced concrete with steel duct in perfect condition
- Reinforced concrete with steel duct with missing grouting
- Reinforced concrete with steel duct with missing grouting and strands
- Reinforced concrete with plastic duct in perfect condition
- Reinforced concrete with plastic duct with missing grouting
- Reinforced concrete with plastic duct with missing grouting and strands
- Steel
- Timber

3. Technical brief

3.1. Simulation environment GEANT4

The simulation of the live environment plays an important role in both detector development and deployment. To simulate the passage of cosmic particles through hidden elements and develop the suitable measurement system, Geant4 software is used. Geant4 (for GEometry ANd Tracking) (Agostinelli) is a platform for "the simulation of the passage of different particles through matter" using Monte Carlo methods. The input to cosmic-ray modelling is taken from the best suited codes, such as CRY cosmic-ray shower generator or Muon Parameterisation Source (MPS).

The CRY software library generates correlated cosmic-ray particle shower distributions at one of three elevations (sea level, 2100 m, and 11300 m) for use as input to transport and detector simulation codes. CRY simulation is based on precomputed input tables derived from full MCNPX (Monte Carlo N-Particle eXtended) transport simulations of primary cosmic rays on the atmosphere and benchmarked against published cosmic-ray measurements.

CRY simulation provides all particle production (muons, neutrons, protons, electrons, photons, and pions) with the proper flux within a user-specified area and altitude. The code generates individual showers of secondary particles sampling the energy, time of arrival, zenith angle, and multiplicity with basic correlations, and has user controls for latitude (geomagnetic cut-off) and solar cycle effects (Figure 1). The distribution shows we can apply the intrinsic scattering angle θ as a discriminating parameter classifying the type and energy range of the hodoscope passing particle. The latter improves the tomographic reconstruction of scanned samples very significantly. The ed areas denote the muon and electron dominated values of θ (blue, yellow) and the mixed region (gray).

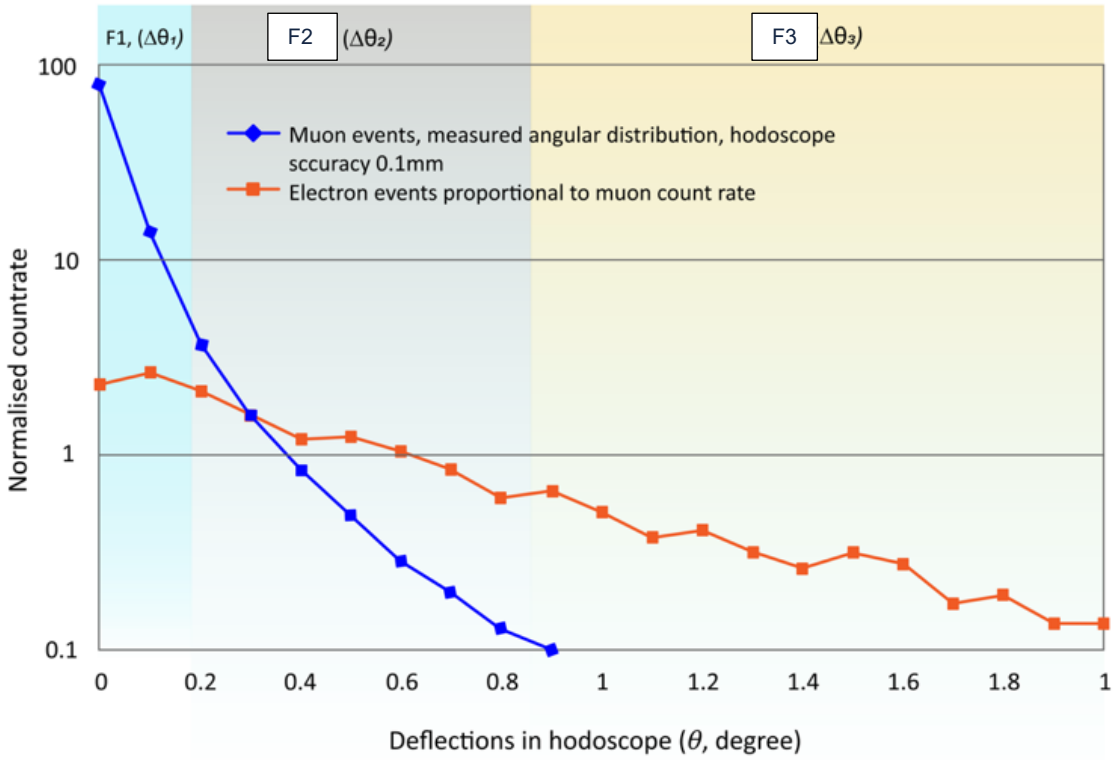

Figure 1. The distribution of atmospheric ray muons and electrons as a function of the intrinsic scattering angle θ in the hodoscope (from the Geant4 model with the CRY event generator).

CRY cosmic ray event generator is used to model the atmospheric ray flux consisting of muons and electrons at sea level. We fixed the spatial resolution of detector plates at 0.1 mm, which corresponds to the angular resolution of 1 mrad for particles approaching the hodoscope

orthogonally. Considering the angular resolution of the hodoscope, the total spectral range presented in Figure 3 can be divided into different numbers of groups - in Figure 3 we have separated the spectrum into the three groups: F1 (dominated by muons), F2 (mixed muons and electrons) and F3 (dominated by electrons).

3.2. Equipment technical specification

In the beginning of 2025, an extensive upgrade to hodoscopes was done. The upgraded system is now capable of performing measurements without an additional PC rack and the scanners have only a power cable that needs to be attached to a 220V socket (Figure 2).

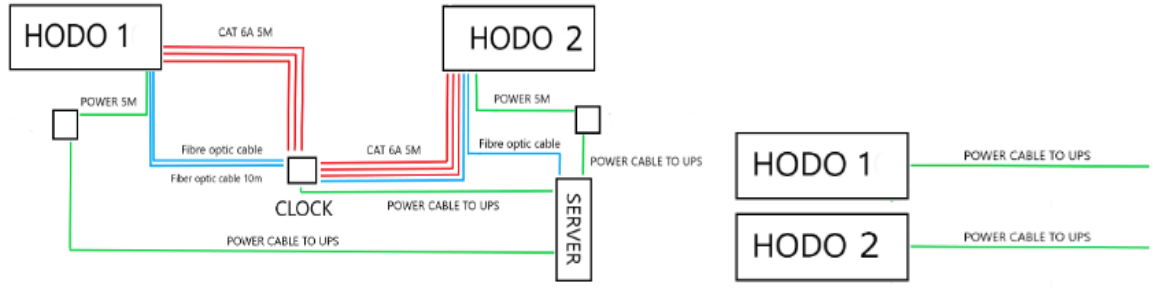

Figure 2. Comparison of old and new generation tomographic scanner setup

The second-generation scanner casing has dimensions of 1715 x 1014 x 381 mm and contains the same sensor plates, which measure 1535.5 x 767.5 mm. The primary hardware enhancement is faster data acquisition; operational availability has also increased from 60% to 90%, and data quality has improved from a 60/40 to an 80/20 data-to-noise ratio. Additionally, tomographic measurements can be performed in a single location with multiple setups, and the measurements are managed through a cloud-based user interface, enabling automated data transfer for post-processing.

The integrated design of the second-generation scanners (Figure 3) has resulted in a combined weight of 94 kg. These scanners utilize a passive cooling system, allowing for operation in ambient temperatures up to 20°C, the active cooling is currently under development, and the casings are already equipped with the necessary ports. The power consumption for each scanner is currently 450W.

Figure 3. Scanner TLL in the production facility

3.3. Data acquisition process

The initial phase of data acquisition takes place directly within the hodoscope itself, ensuring a streamlined and efficient handling of raw sensor data. This stage is comprised of three key steps:

1. **Raw Data Acquisition:** This foundational step involves the immediate collection of raw data from the hodoscope's sophisticated array of sensors. This raw data constitutes the fundamental information regarding the characteristics and behaviour of particles or radiation as they traverse the detector. It is the unfiltered input upon which all subsequent analyses are built.
2. **Data Preprocessing and Calculation of Internal Coordinates:** Following raw data acquisition, a crucial preprocessing stage is initiated. During this phase, the raw data undergoes rigorous filtering to eliminate inherent noise and correct for any biases specific to the hodoscope's detector components. Concurrently, relevant features are meticulously extracted from the refined data. A particularly vital aspect of this step is the precise calculation of internal coordinates within the hodoscope's detection volume, derived directly from the sensor readings. These meticulously calculated coordinates are essential for accurately reconstructing the trajectories of the particles, providing the spatial context for their movement.
3. **Data Streaming to Cloud:** Once the data has been pre-processed and its internal coordinates calculated, it is then efficiently streamed to the cloud for more extensive and computationally intensive analysis. To ensure optimal bandwidth utilization and minimize transmission times, the data is typically compressed before transmission. This compression is a critical step in maintaining the system's overall efficiency.

By executing these initial processing steps directly on the hodoscope device, the system achieves several significant advantages. Foremost among these is a substantial reduction in the volume of data that needs to be transmitted to the cloud, which in turn minimizes network latency and conserves valuable bandwidth. Furthermore, this in-hodoscope processing capability enables the system to adapt in real-time to changing environmental conditions. This real-time adaptability is facilitated by the continuous collection and export of performance

metrics directly from the device, allowing for immediate adjustments and optimizations. Cloud Processes: Advanced Analysis and Visualization

The second phase of data acquisition and analysis leverages the distributed computing power of the cloud to perform more sophisticated operations that are beyond the capabilities of the hodoscope device alone. This stage also consists of three distinct steps:

1. **Data Real-Time Processing:** Upon its arrival in the cloud, the pre-processed data undergoes further real-time processing. This cloud-based processing can accommodate more computationally intensive algorithms that are not practical to execute on the hodoscope device itself. This allows for a deeper and more nuanced analysis of the collected data.
2. **Reconstruction and Object/Material Detection:** The extensively processed data is then utilized to meticulously reconstruct the intricate trajectories of particles as they passed through the hodoscope. Building upon these highly accurate reconstructed trajectories, the system can then effectively detect and precisely identify various objects or materials present within the scanned volume. This capability is central to the system's primary function of environmental or object analysis.
3. **Results and Metrics Visualization:** The culmination of the entire data acquisition and analysis pipeline is the comprehensive visualization of the results. This includes highly detailed visualizations of reconstructed particle trajectories and clearly identified objects or materials, all presented in a manner that provides users with immediately actionable insights. In addition, a wide array of performance metrics related to the hodoscope's operational status, the efficiency of the cloud infrastructure, and the overall quality of the acquired data are continuously monitored. This continuous monitoring is paramount to ensuring the sustained optimal performance of the entire system and identifying any potential issues proactively.

The integration of cloud-based processing empowers the system to employ more sophisticated analytical techniques and advanced visualization methods, capitalizing on the immense power of distributed computing resources. Moreover, the diligent and continuous monitoring of both system and data quality plays a pivotal role in the early identification of potential issues, thereby contributing significantly to an overall improvement in measurement accuracy and operational efficiency. This synergistic approach between in-hodoscope and cloud processes ensures a robust, efficient, and highly capable data acquisition and analysis system.

4. Development

4.1. Human resources assignment and roles

Table 1. Human resources

	Affiliation	Role	Contact info (mail)
Sander Sein	GSCAN	Supervision	Sander.sein@gscan.eu
Sander Möller	GSCAN	Preparation of the MFT measurement platform	Sander.moller@gscan.eu
Christyna Hrytsiuk	GSCAN	Simulation study	Christyna.hrytsiuk@gscan.eu
Mikhail Iljin	GSCAN	Calibration measurements	Mikhail.iljin@gscan.eu

4.2. Scheduling

T2.4.1 Design basis of methodology and performance analysis (M3 to M7)

T2.4.2 Simulation study (M5 to M10)

T2.4.2 Improvements to data collection and interface (M7 to M14)

T2.4.4 Real material validation measurements (M10 to M17)

T2.4.5 Report writing and review (M14 to M17)

	2024					2025									
	Aug	Sep	Oct	Nov	Dec	Jan	Feb	Mar	Apr	May	Jun	Jul	Aug	Sep	Oct
	M3	M4	M5	M6	M7	M8	M9	M10	M11	M12	M13	M14	M15	M16	M17
T2.4.1															
T2.4.2															
T2.4.3															
T2.4.4															
T2.4.5															

4.3. Critical tasks and milestones

4.3.1. Critical Tasks

Task and contigency	Probability	Impact
T2.4.2 Simulation study will not be according to the real environmental measurements. The measurement scenarios will be overlooked in T2.4.1	Low	Low
T2.4.3 Improvements are done based on theoretical information and not real situation. The testing involves more than five personas and interface can be adjusted during T11.2.	Med	Med
T2.4.4 Different testing materials are not available for verification. Materials are prepared and ordered before the beginning of the task	Med	Med

4.3.2. Milestones

- AI models for material detection in the field (M17)

Verification form: Algorithms and laboratory results (D2.1 to 2.6) completed.

D2.4 (together with the other WP2 deliverables) ensures that there is sufficient data on which to train and test the WP3 AI algorithms. Thus, the complementation with open datasets ensures the smooth operation of WP3 and of the project.

4.4. Simulation study

For statistical analysis, 2D GEANT4 geometries were created and simulated with up to 10,000 particles, classifying results by energy, charge, and number. Average refraction and standard deviation were used for analysis. The most effective energy range is 0.5 to 3.0 GeV, where refraction is clearest. Distinctions are possible after only 100 particle traversals, indicating faster measurements with prior knowledge.

Twenty 1 m³ simulation geometries were created, with 18 showing visual differences. A vertical CRY (muons with natural energy distribution) beam was used. Although the approximate muon energy is 4 GeV, muons were divided into five energy classes:

- 0.0-0.5 GeV,
- 0.5-1.5 GeV,
- 1.5-3.0 GeV,
- 3.0-10.0 GeV,
- 10.0-maximum GeV.

1,000,000 events were simulated per case; mean, median, and standard deviation were estimated.

Initial analysis showed significant muon scattering angle variation, highlighting the need for sufficient statistics. Mean scattering angles can classify muons based on their energy-dependent scattering angles (Figure 4). The mean scattering angle for plain concrete is 74.29 rad and with rebar 77.95 rad, which is above the tracking accuracy of 0.01 rad.

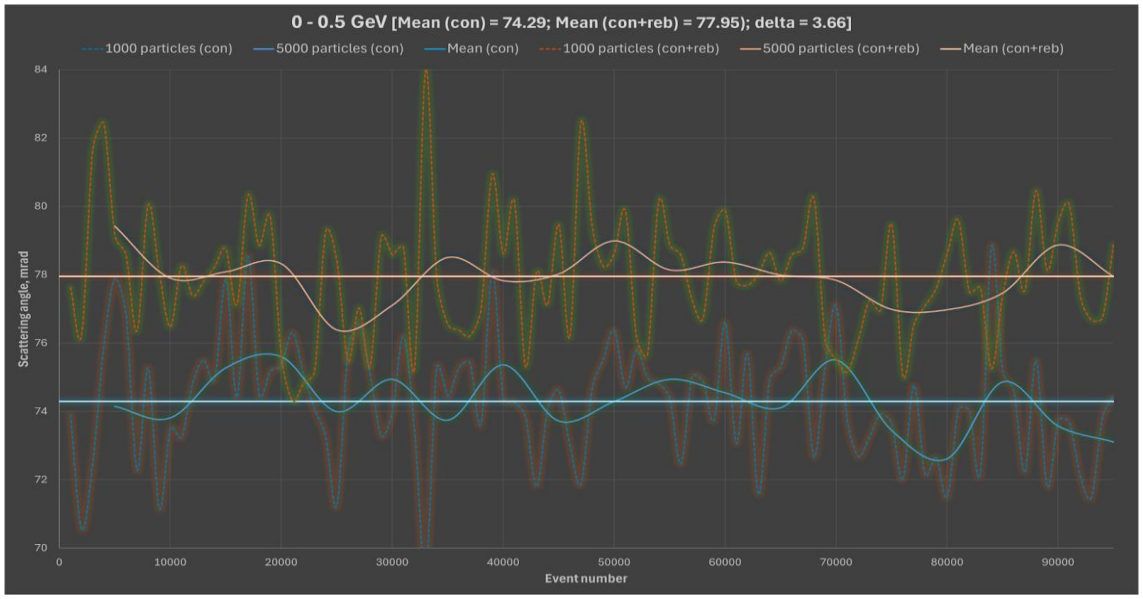

Figure 4. Scattering angle distribution of 0 – 0,5 GeV muons through plain concrete and concrete with 10 mm rebar.

To determine the smallest detectable rebar and rust, two cases based on concrete thickness and scattering angle differences were investigated (Figure 5).

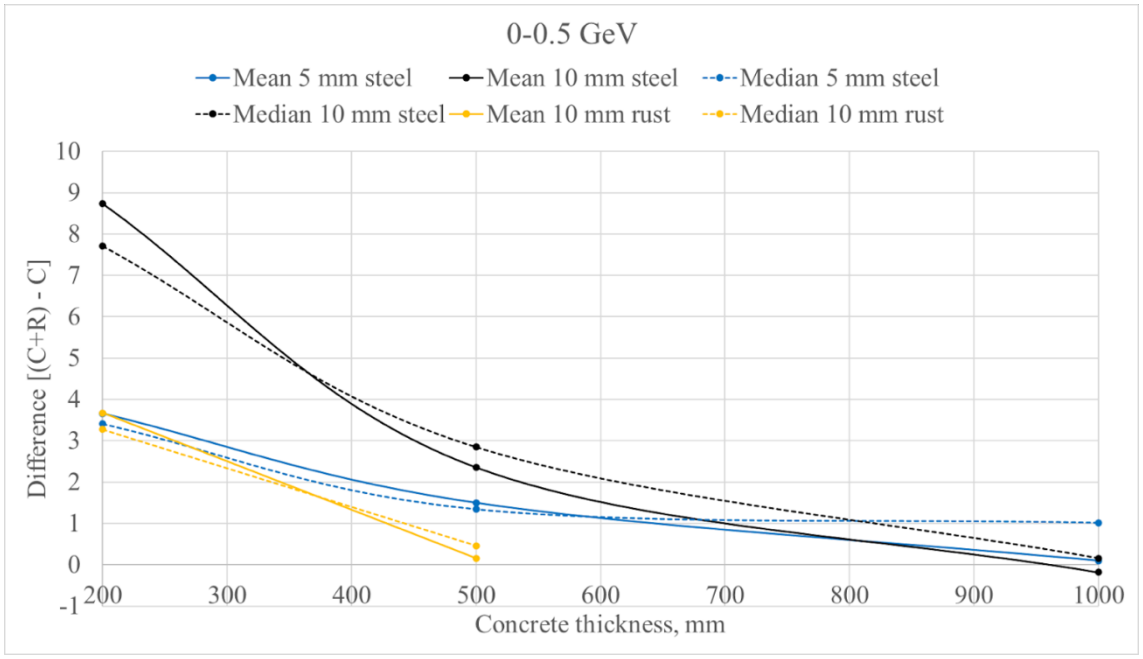

Figure 5. Scattering angle differences of 0 – 0,5 GeV muons through plain concrete, concrete with 10 mm rebar, 10 mm rebar with 5 mm rust and fully rusted.

Low-energy muons can detect corrosion in concrete up to 420 mm thick and 5 mm rebar in concrete over 700 mm thick. Medium-energy (1.5-3.0 GeV) muons cannot detect corrosion or 5 mm rebar but can detect 10 mm rebar in bodies up to 380 mm thick. Very high-energy (3.0+ GeV) muons scatter too little for small element distinction. Summary figures (Figure 6, Figure 7, Figure 8) generalize based on 1,000,000 particles for 500 mm thick concrete.

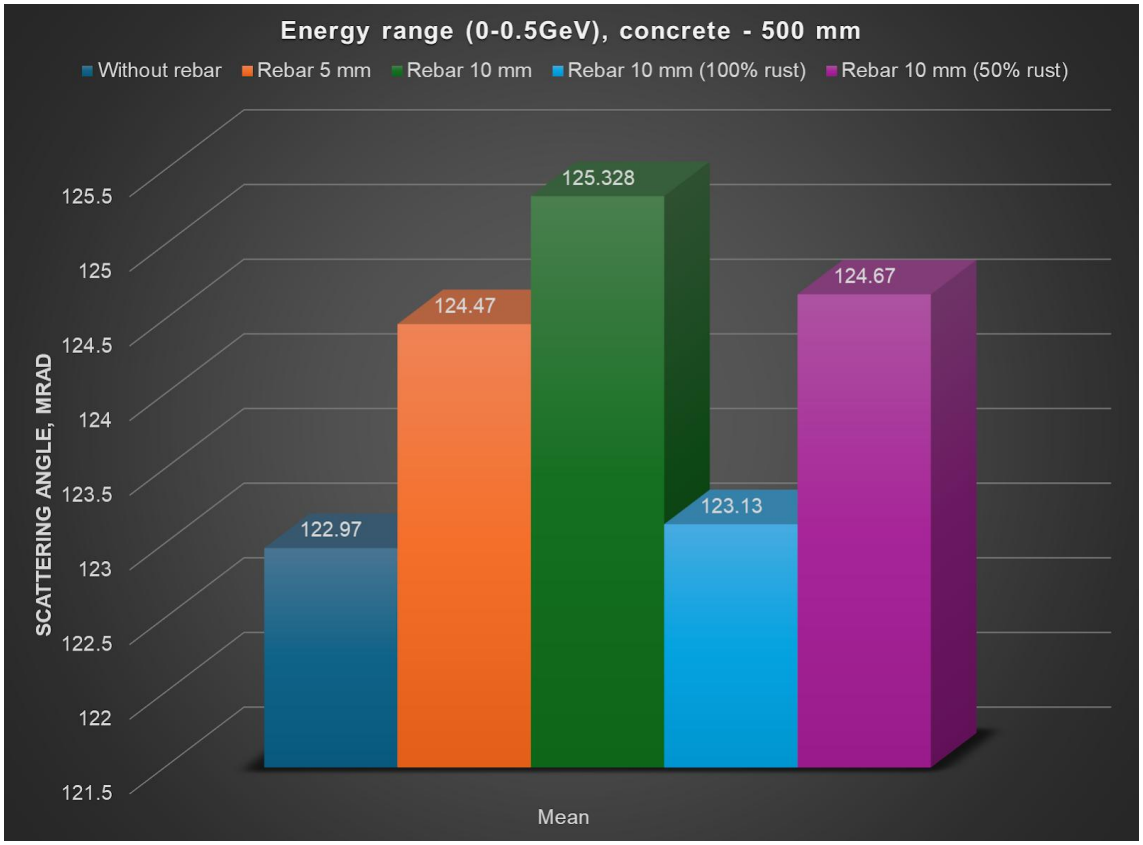

Figure 6. Scattering angle differences of 0 – 0.5 GeV Muons in 500 mm block

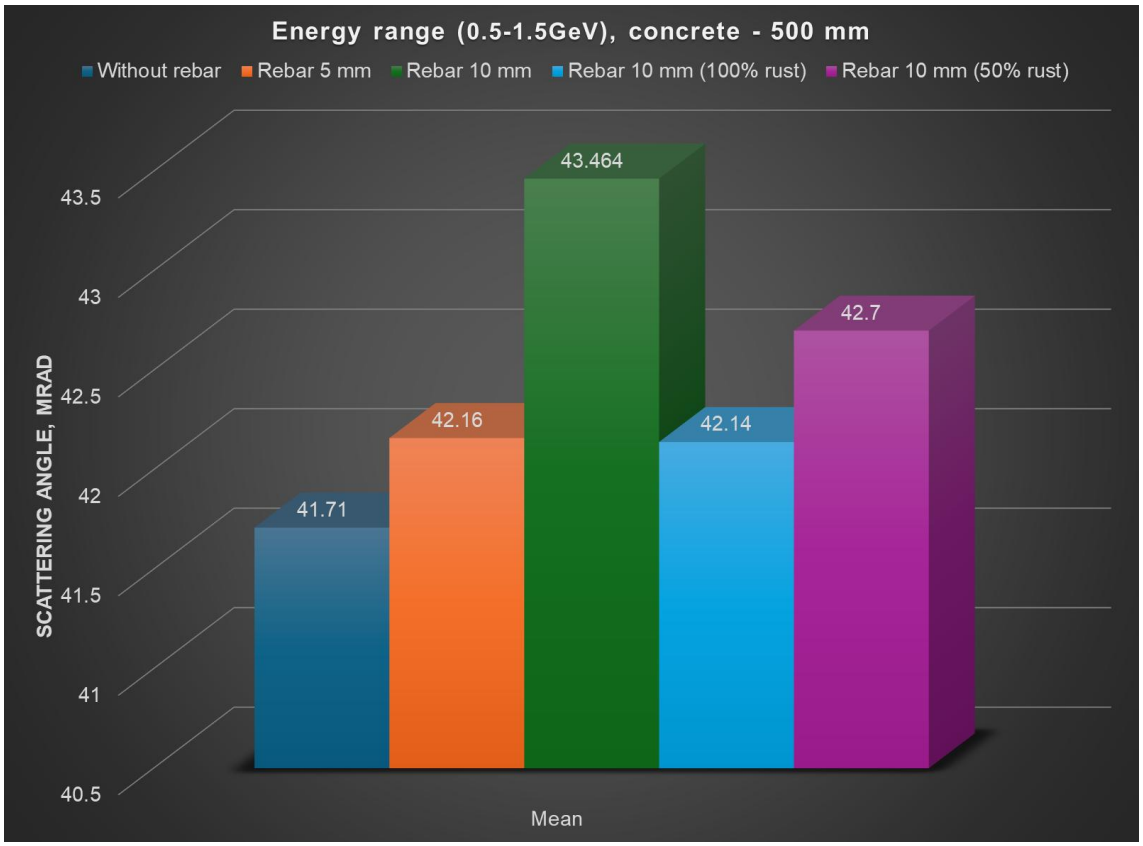

Figure 7. Scattering angle differences of 0.5 – 1.5 GeV Muons in 500 mm block

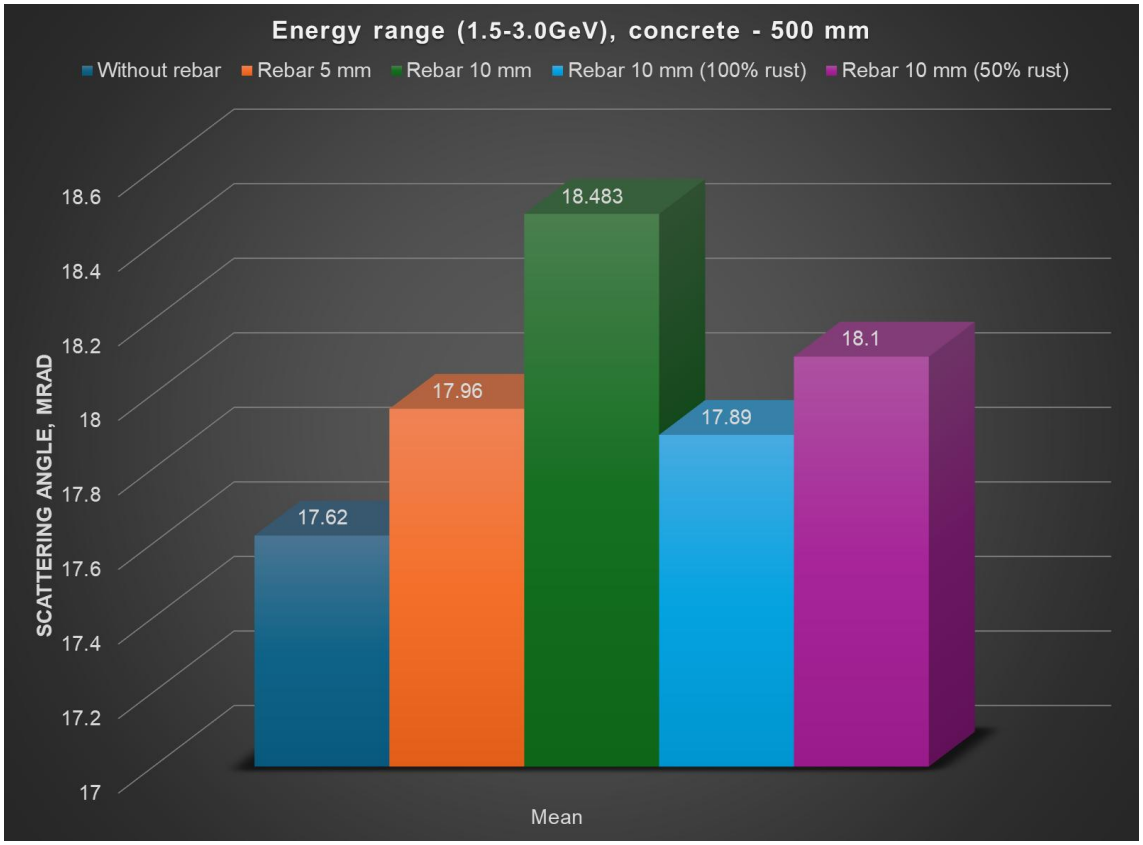

Figure 8. Scattering angle differences of 1.5 - 3.0 GeV Muons in 500 mm block

The lowest energy range shows clear scattering distinctions in all scenarios. In higher ranges, for a 500 mm thick body, the difference between unreinforced and 5 mm reinforced cases is too small. Any larger internal element and concrete voids starting from 5 mm are detectable.

The influence of concrete carbonation (Papadakis) and chloride penetration on muon scattering was also analysed. A literature review identified hydrogen/carbon changes for carbonation and sodium/chlorides for chloride penetration (Table 2).

Table 2. Chemical composition of CEM I plain concrete and change of composition for different degradation processes

Chemical element	Initial quantity	Carbonisation	Chloride ingress
H	0.01	**0.005523**	0.009956
C	0.001	**0.004662**	0.000996
O	0.52911	0.526273	0.526792
Na	0.016	0.016127	**0.017653**
Mg	0.002	0.002016	0.001991
Al	0.03387	0.034139	0.033722
Si	0.33702	0.339696	0.335544
K	0.013	0.013103	0.012943
Ca	0.044	0.044349	0.043807
Fe	0.014	0.014111	0.013939
Cl	0	0	**0.002657**
Total	1	1	1

Carbonation is detectable in the two lower energy ranges, but chloride penetration (at FIB's 2% limit) is with less than 1 mrad mean scattering angle difference in detection (Figure 9).

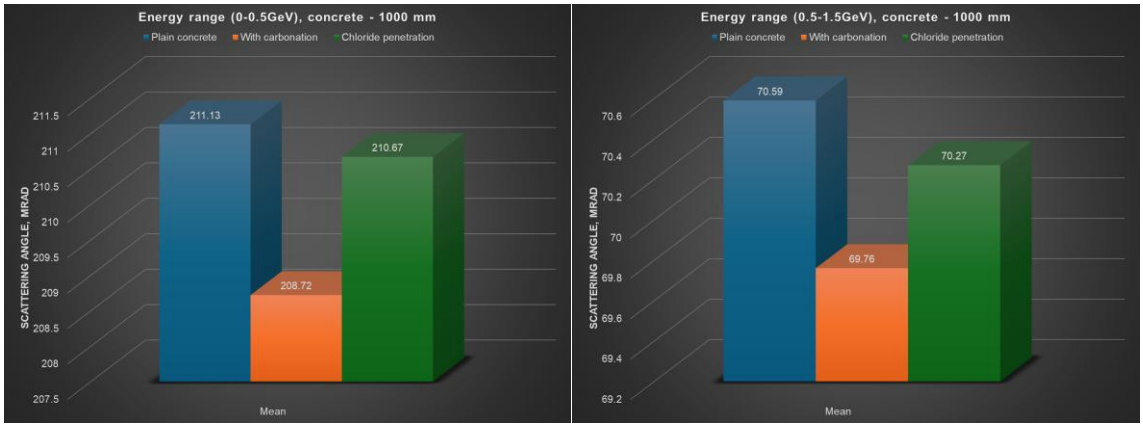

Figure 9. Scattering angle differences of 0-0.5 and 0.5 - 1.5 GeV Muons in 1000 mm block with different degradation processes.

To use the technology for degradation process detection, the detection should be less than 0.5 mrad.

In addition to mean scattering angle investigation the potential measurement time to detect steel rebars were carried out.

Based on the simulation study, it is possible to detect rebar with 24-hour measurement (Figure 10 left), but determination of the accurate diameter is challenging. 72-hour measurement yields clearer shapes,120-hour measurement (Figure 10 right) highlights concrete body shape and improves rebar distinction from the side. 168-hour measurement allows clear rebar distinction and diameter measurement.

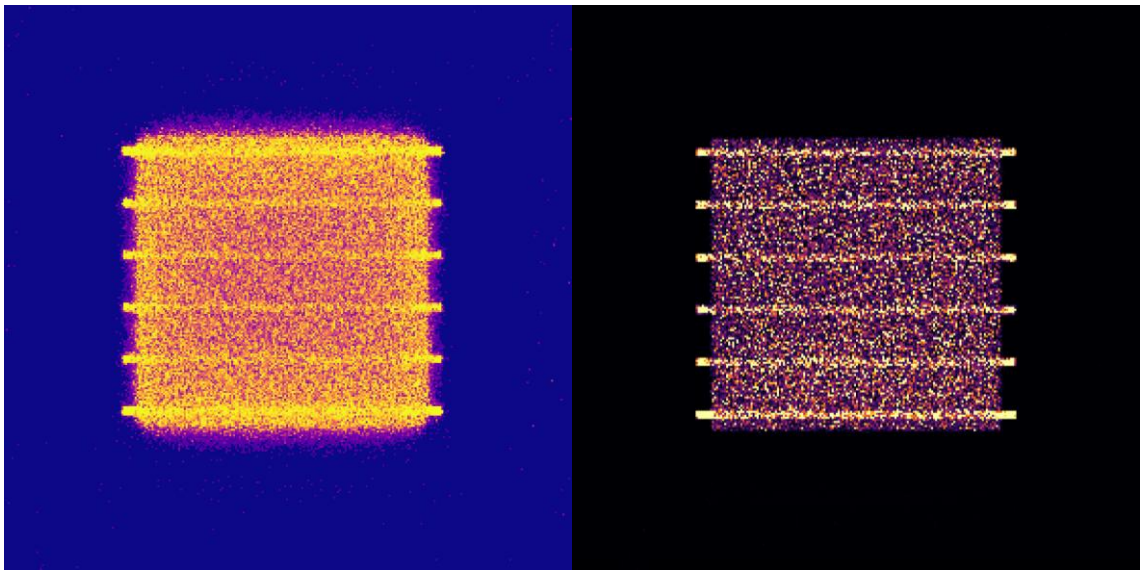

Figure 10. Rebars in 1000 thick concrete block after 24 h (left) and 120 h (right) exposure time

Simulations show that with 5 mm resolution and 24-hour measurement, elements and defects in a cubic meter body are distinguishable.

Optimal horizontal measurement time is 120 hours in perfect conditions and for 3 mm voxel resolution. these needs increasing for vertical measurement and can be reduced for smaller objects.

4.5. Real material testing with respect to application and utilization

Since the experiments need to be conducted in controlled conditions and for known materials (Ground Truth) a separate scanner setup was prepared to minimise the errors from scanner positioning (Figure 11).

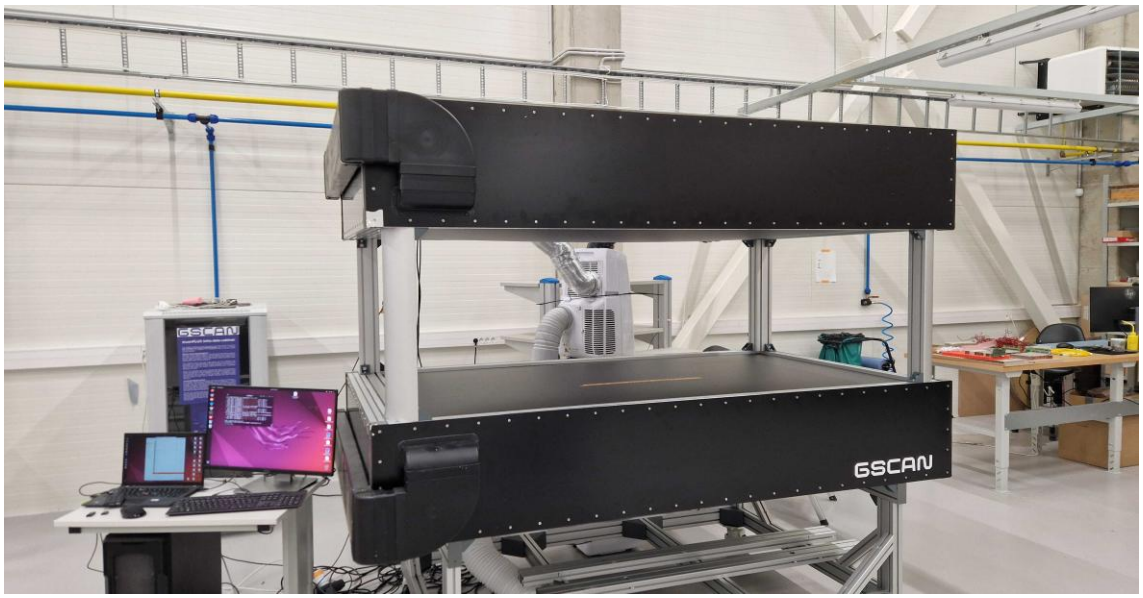

Figure 11. Scanner setup for material validation

The measurements started with just air measurements (Figure 12) to understand the general muon flux in the location and normalize the initial environment.

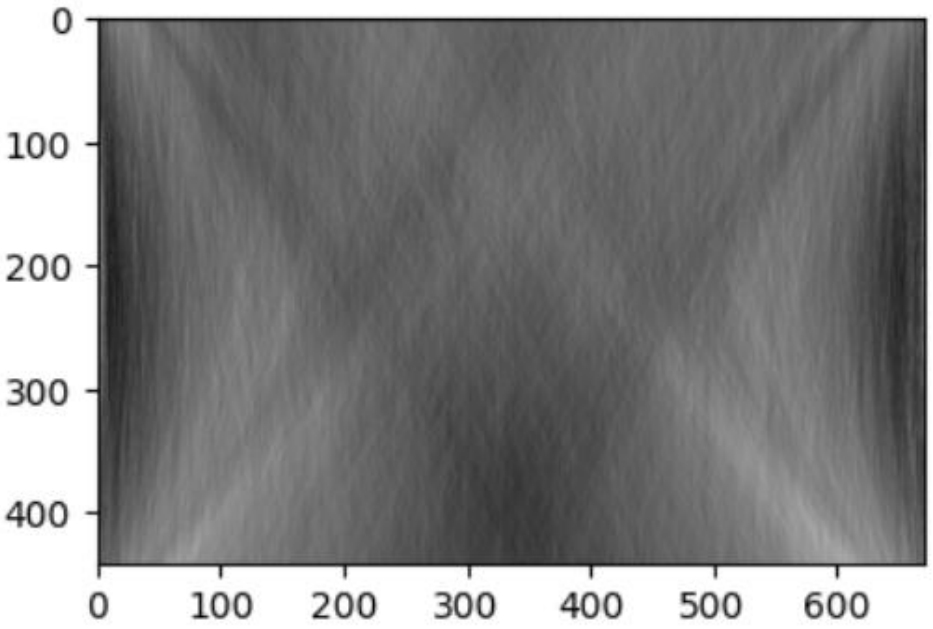

Figure 12. Air measurements with rhombus shape, which reflects how the muon flux filtering cuts of specific energy levels in reconstruction algorithm.

The air measurements revealed the change of flux in different angles and how the cut off filter for electronics work – lower energy particles with higher scattering in air are removed.

First experiments with materials were conducted in as simple environments as possible, scanning only on object at a time for five consecutive days (120 h). All the measurements were

repeated with slightly changed positioning of materials. The first measurements included concrete and steel with variations in size – either 100 mm cubes or 150 mm cubes (Figure 13, Figure 14, Figure 15).

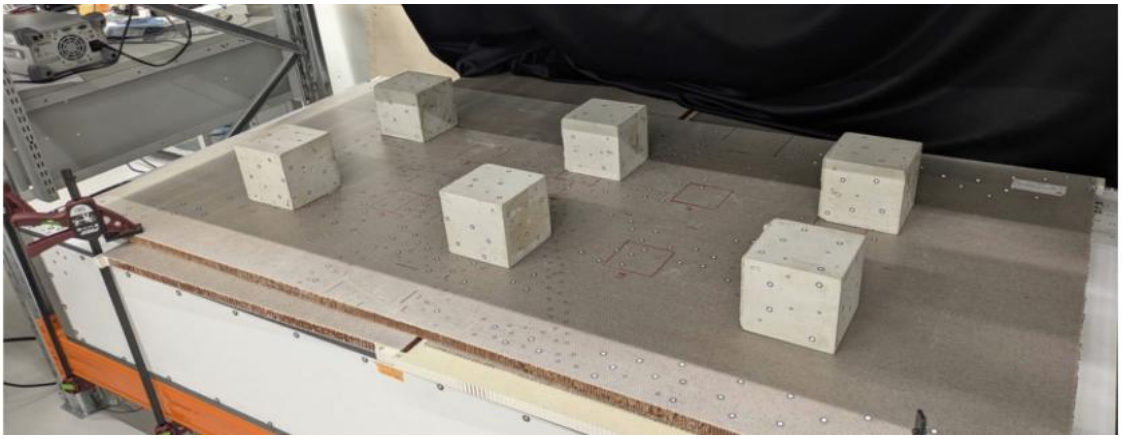

Figure 13. Six concrete cubes in a measurement setup. Experimental run number 17

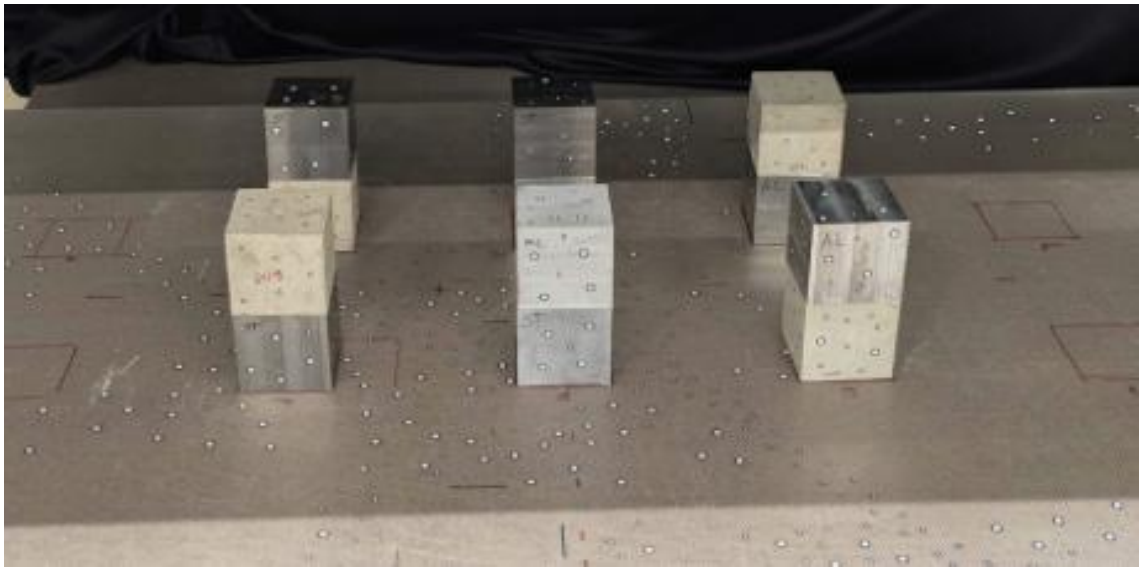

Figure 14. Twelve cubes stacked on top of each other with steel and concrete in a measurement setup. Experimental run number 14

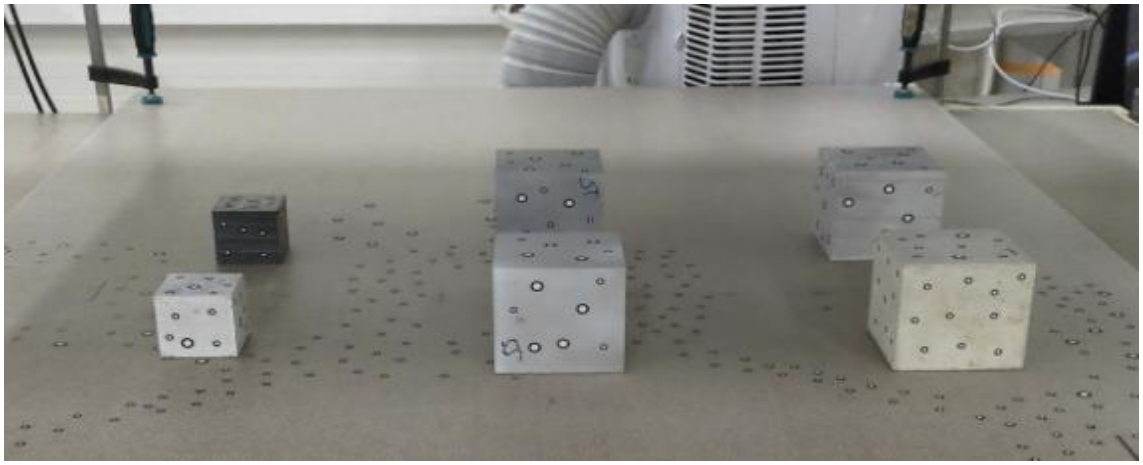

Figure 15. Mix of six cubes of different sizes of concrete and steel in a measurement setup. Experimental run number 13

Even the raw reconstruction results reveal the difference of scattering density (Figure 16).

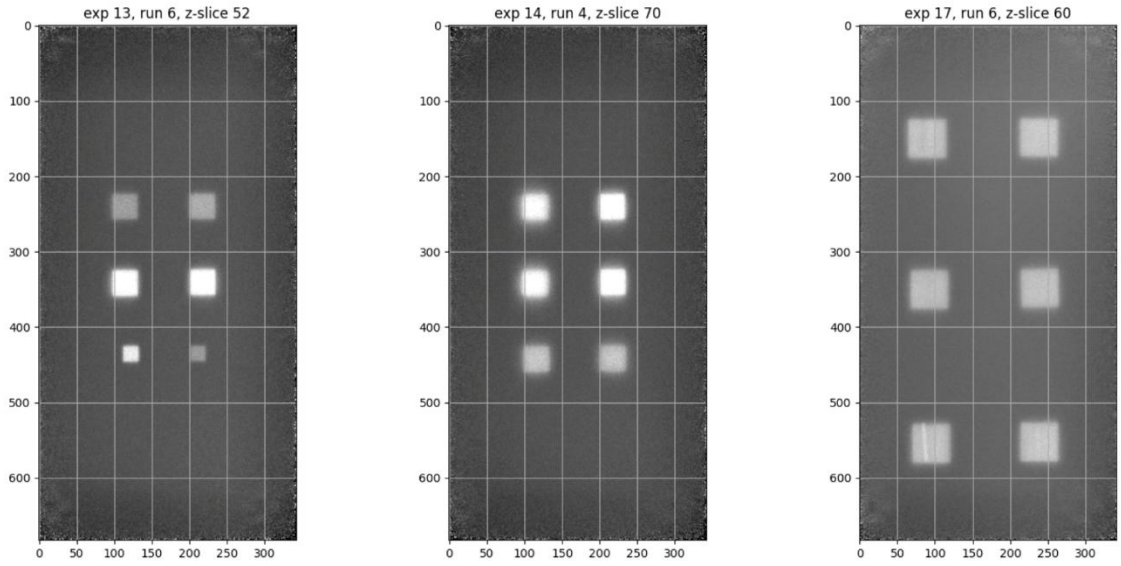

Figure 16. Reconstruction results of the measurement setups. Where steel with higher density appear brighter, because it is causing more scattering.

With small elements and solid materials, the simulation study results were verified. The research continues with more complex and advanced reconstruction and material classification algorithms.

The more complex measurements where timber, steel or concrete test bodies were mixed, started also with separate positioning (Figure 17).The focus was to get statistically significant results that will allow to decrease the measurement time in long term.

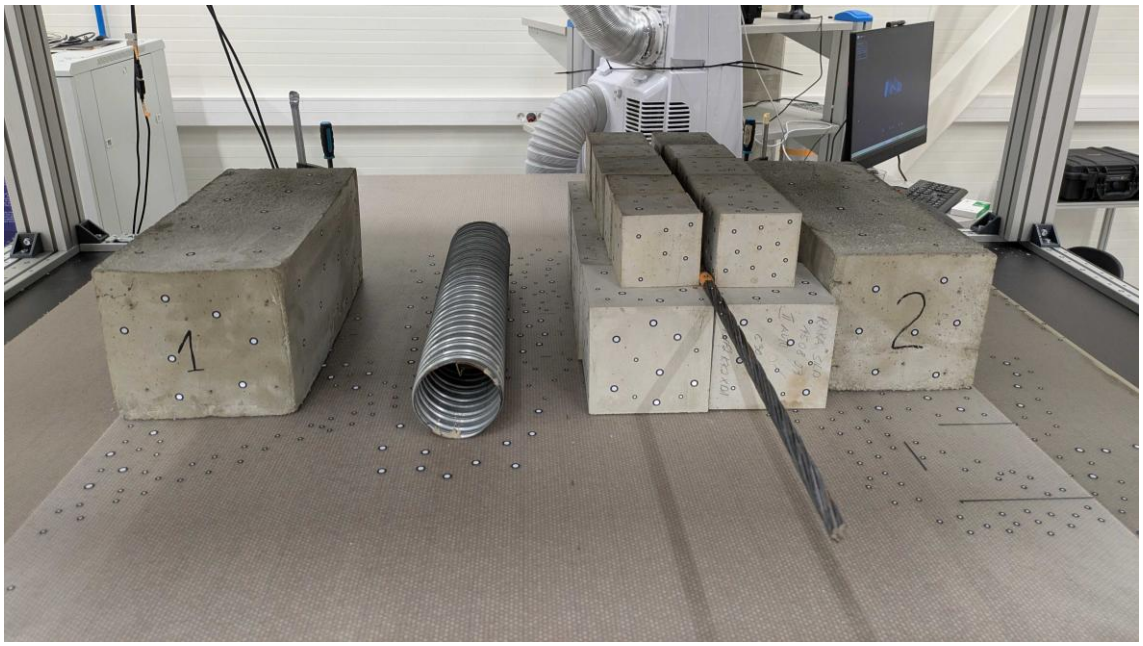

Figure 17. Measurement setup with composite and more complex variations of materials. Larger test bodies nr. 1 and 2. have both rebars and post-tensioning ducts inside.

The raw reconstruction results also reveal the change of densities and scattering (Figure 18).

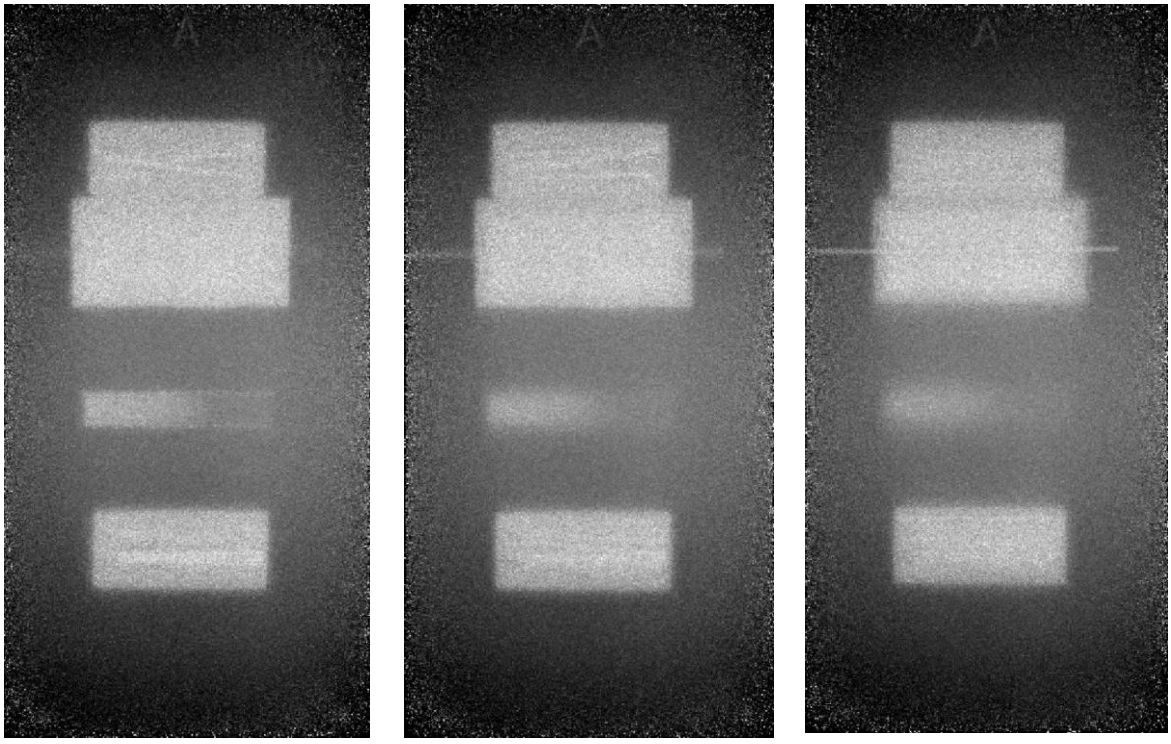

Figure 18. Horizontal slice from different heights of the measurement of composite and more complex variations of materials.

The verification measurements and all the findings show that developed tracking, alignment and reconstruction algorithms are effective.

5. Challenges and limitations

MFT is relatively new technology in the field of structural assessment which causes challenges related to reliability and usability due to lack of standardized procedures and stakeholders not being aware of the possibilities.

5.1. Technical constraints of the technology

The technology has many technical constraints that can be divided to hardware, data acquisition and data processing related issues. The first deliveries of real structural elements in 2024 identified and visualized the internal mechanics of post-tensioning ducts, separating grouting and strands. Object detection differentiated individual ducts for condition assessment, detecting duct strands, grouting, voids, and corrosion (Figure 19). Material clustering quantified missing grouting, strands, and potential corrosion. Findings were presented in 2D. Machine learning improved duct area condition classification, and the GScan reconstructive algorithm enhanced reconstruction images.

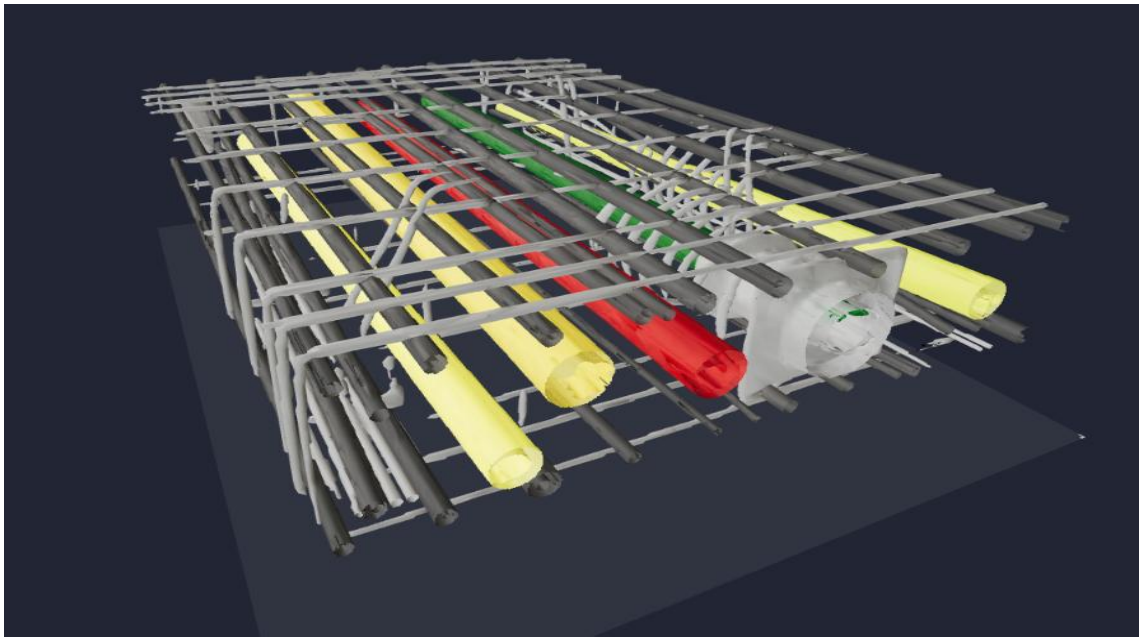

Figure 19. The outcome of the MFT data

5.1.1. Hardware

The main goal of the hardware is to track the muons as efficiently as possible, but the efficiency is related to detector area and data acquisition electronics.

- Larger detectors are more efficient, but the weight and size causes problems with accessibility and to logistics.
- The fibre size 0.9 mm limits the tracking accuracy to 0.1 mm and 1 mrad, which means that smaller differences in materials can't be detected.
- Data readout electronics need continuous power that is at least 450 W. This limits the possibility to perform measurements in remote areas.
- Data readout electronics produce heat that causes noise in measurement data and limits the operational temperature to 20 degrees.

5.1.2. Data acquisition

The well-established data acquisition enables the possibility to perform measurements faster and monitor the equipment.

- For most of the common structures, the measurement time is at least 10 days, which limits performing the measurements in public places or on the roads with heavy traffic. Vertical measurements extend the measurement time up to 10 times.
- The cloud system needs at least 4G internet connection that is difficult to obtain in remote areas and inside buildings.
- The tomographic setup need access to at least two sides of the structure.
- The scanners need to be on a stable ground and as close as possible to the area of interest.

5.1.3. Data processing

Data processing involves the data improvement, reconstructions, object detection, material classification and output to external software.

- Development maturity is limited to performed simulations and measurements. Every new use-case needs manual processing and verification.
- The data reliability is validated with non-statistical methods, which allow to provide results with uniform distribution. More measurements are needed for statistical uncertainty assessment.

- Algorithms development is very rapid and almost every week, there are new findings which disables to standardize the procedures.
- The data output into different formats is limited due to missing framework and clear data interpretation needs.

6. Conclusion

This deliverable successfully outlines the development and validation of MFT for data collection from complex and concealed elements, fulfilling the objectives of Task 2.4.

Through rigorous GEANT4 simulations and real material testing, the efficacy of the developed tracking, alignment, and reconstruction algorithms has been verified. The simulation studies demonstrated the potential to detect internal elements and degradation processes, with optimal measurement times identified for various resolutions and object types.

Real material testing further validated these findings, showing clear distinctions in scattering density for concrete and steel. While challenges related to hardware limitations, data acquisition time in public areas, and the need for continuous internet connectivity persist, the technology's ability to provide unique 3D data for hidden elements significantly contributes to the overall SUM4Re project goals.

The deliverable concludes with actionable recommendations to address identified challenges, optimize data collection, and ensure alignment with the broader objectives of SUM4Re, particularly in supporting the training and testing of WP3 AI algorithms and contributing to C-BIM models for WP6 and the Netherlands case study in WP10.

7. Bibliography

Agostinelli, S., Allison, J., Amako, K. A., Apostolakis, J., Araujo, H., Arce, P., ... & Geant4 Collaboration. (2003). Geant4—a simulation toolkit. Nuclear instruments and methods in physics research section A: Accelerators, Spectrometers, Detectors and A. *Test*. Test: Test, 2024.

GEORGADZE, A., KIISK, M., AVOTS, E., & Anbarjafari, G. (2023). U.S. Patent No. 11,774,626. Washington, DC: U.S. Patent and Trademark Office. n.d.

Geraldo, B., Vicente, R., Ferreira, R. J., Goes, M. M., & Marumo, J. T. Characterization of filter cartridges from the IEA-R1 reactor by radiochemical method. *Test*. Test: Test, 1985.

Jol, H. M. (Ed.). (2008). Ground penetrating radar theory and applications. elsevier. n.d.

Niederleithinger, E., Gardner, S., Kind, T., Kaiser, R., Grunwald, M., Yang, G., ... & Mahon, D. (2021). Muon tomography of the interior of a reinforced concrete block: First experimental proof of concept. Journal of Nondestructive Evaluation, 40(3), 65. n.d.

Papadakis, V. G., Vayenas, C. G., & Fardis, M. N. (1991). Fundamental modeling and experimental investigation of concrete carbonation. Materials Journal, 88(4), 363-373. n.d.

SEIN, S., KIISK, M., MÄGI, M., & TARK, K. (2025). Applications of Muon Flux Tomography in assessment of civil engineering structures. n.d.

SUM4Re

Creating materials banks
from digital urban mining

Funded by the European Union. Views and opinions expressed are however those of the author(s) only and do not necessarily reflect those of the European Union. Neither the European Union nor the granting authority can be held responsible for them.

Funded by
the European Union

SUM4Re

Creating materials banks
from digital urban mining

www.sum4re.eu sum4re@uvigo.gal SUM4Re SUM4Re_EU

Funded by the European Union. Views and opinions expressed are however those of the author(s) only and do not necessarily reflect those of the European Union. Neither the European Union nor the granting authority can be held responsible for them.

Funded by the European Union